EurJIC
European Journal of Inorganic Chemistry

Research Article
doi.org/10.1002/ejic.202500203

Chemistry Europe
European Chemical Societies Publishing

www.eurjic.org

Following the In Situ Pathway of Photoactivated Cyclopentadienone–NHC Iron Complexes as Ammonia–Borane Dehydrocoupling Bifunctional Catalysts

Andrea Cingolani, Nicola Schiaroli, Carlo Lucarelli,* Chiara Lenzi, Andrea Masetti, Cristiana Cesari, Francesca Forti, Stefano Zacchini, Jacopo De Maron, Francesco Luca Basile, and Rita Mazzoni*

Carbonyl iron complexes, bearing cyclopentadienone/hydroxycyclopentadienyl ligands and N-heterocyclic carbene as noninnocent and ancillary ligands, are active as ammonia–borane dehydrocoupling catalysts under photoactivation conditions. Dehydrogenation occurs at room temperature and is complete (in NMR tube) after 2 h with 10 mol% of cationic complex **2**, and after 4 h at lower catalytic loading (2 mol%) with the preactivated form **3**. Reaction coproducts have been identified by ^{11}B-NMR. The reaction crudes reveal mixture of borazine and corresponding crosslinked polymer, together with other linear/branch polyaminoboranes for **1** and **2,** and insoluble polyaminoboranes under even milder conditions (no irradiation) for **3**. Scale-up of the reaction in a photoreactor then allows to quantify the catalysts activation, measuring CO release, as well as their productivity in term of H_2 produced. The in situ IR analysis sheds light on the different mechanistic pathways followed by the neutral **1** and the cationic **2** precatalysts. As a general statement, **2** is both easier to be activated and more efficient than the neutral counterpart **1**. Preactivation of catalyst **2**, replacing a CO with a more labile CH_3CN leading to complex **3,** is exploited to improve the reaction speed and further explore the reaction mechanism.

1. Introduction

Hydrogen, a versatile energy carrier, is one of the key solutions envisioned to unlock a future independent of fossil fuels, with low or even negative carbon dioxide emissions. However, replacing storage methods in these sectors and using hydrogen as an energy carrier can help address various energy challenges, including in hard-to-decarbonize industries such as aviation, shipping, and chemical production. Despite this, creating a new hydrogen value chain based on solid and liquid hydrogen storage remains one of the significant challenges of our time. To address this, numerous global initiatives have been launched to accelerate the development and scaling up of hydrogen technologies. In Europe, the European Hydrogen Strategy, alongside REPowerEU, has set a target of producing and importing 10 million tons of hydrogen by 2030.[1] Moreover, through the Mission Innovation,[2] there is an aim to reduce hydrogen production costs to make it competitive with fossil fuels. In this context, the US Department of Energy plans to reduce hydrogen costs from the current 5 dollars per kg to just 1 dollar per kg within the next decade.[3] Overall, an investment of up to 750 billion dollars is expected for the development of the project announced through 2030.[4] While hydrogen production from electrolyzers is paving the way for expanding hydrogen infrastructure, it is also critical to develop alternative production methods to diversify feedstocks and address areas where green electricity and clean water are limited. In this context, the use of ammonia–borane (AB)-derived feedstocks can still play a crucial role as documented by a new proliferation of publications in the field,[5] while awaiting the development of efficient regeneration processes from the dehydrogenation byproducts, which remain one of the main obstacles to the practical application of AB as a hydrogen storage solution.[6]

In principle, ammonia−borane ($H_3N{-}BH_3$, AB) can release ≈19.6% by weight of H_2, which is essentially equivalent to the removal of 3 equivalents of molecular H_2 from AB.[7] In the context of AB chemistry, dehydrogenation leads to the formation of $H_2N{=}BH_2$ (AOB), which then undergoes immediate oligo-polymerization.[8]

A. Cingolani, C. Lenzi, A. Masetti, C. Cesari, F. Forti, S. Zacchini, J. De Maron, F. L. Basile, R. Mazzoni
Dipartimento di Chimica Industriale "Toso Montanari"
Università di Bologna
via Gobetti 85, 40129 Bologna, Italy
E-mail: rita.mazzoni@unibo.it

N. Schiaroli, C. Lucarelli
Dipartimento di Scienza e Alta Tecnologia
Università dell'Insubria
Via Valleggio, 11, 22100 Como, Italy
E-mail: carlo.lucarelli@uninsubria.it

C. Lenzi, A. Masetti, C. Cesari, F. Forti, S. Zacchini, J. De Maron, F. L. Basile, R. Mazzoni
Center for Chemical Catalysis–C3
University of Bologna
via Gobetti 85, 40129 Bologna, Italy

Supporting information for this article is available on the WWW under https://doi.org/10.1002/ejic.202500203

Research Article
doi.org/10.1002/ejic.202500203

Chemistry Europe
European Chemical Societies Publishing

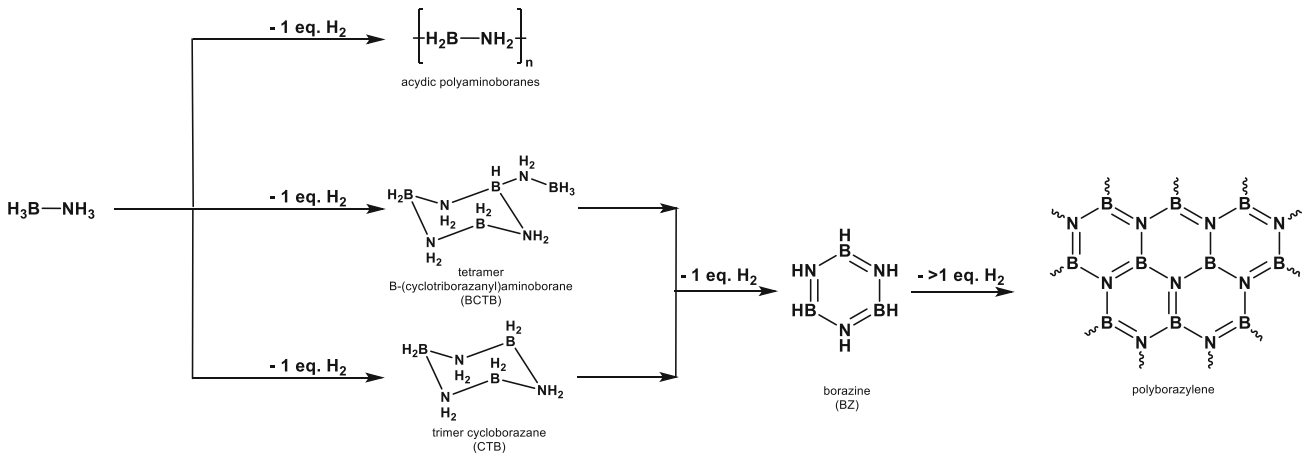

Scheme 1. Major byproducts of dehydrocoupling of AB.

Depending on the reactivity of the metal catalyst, either 1 equivalent or more than 1 equivalent of H_2 per mole of AB can be released, resulting in the formation of several byproducts (**Scheme 1**, e.g., BDCB, CTB, borazine, and insoluble polyaminoboranes). To differentiate between the various behaviors, the catalysts have been classified into two main groups: Type I, which release 1 equivalent of H_2 and are selective toward insoluble polyaminoboranes, and Type II, which can release more than 2 equivalents of H_2, leading to the formation of cyclic products, borazine, and polyborazylenes.[9,10]

Several studies within this field have examined homogeneous catalysts, ranging from noble metals (e.g., Ir and Ru) to earth-abundant ones (e.g., Fe, Co, Mn, and Ni). These studies, combining experimental work, characterization, and density functional theory (DFT) calculations, have advanced the understanding of AB dehydrogenation under mild conditions.[11]

Concerning the most abundant and less toxic one, various homogeneous iron catalysts have been found active in the dehydrogenation of AB. H_2 production range is from 1 to 2.5 eq. and with variable catalyst loading down to 0.5 mol%.[12] Among them the first Fe-based catalyst active, an iron(II) trimethylphospine hydride, Fe(H)–(CH_2PMe_2)–$(PMe_3)_3$, was reported to work at room temperature by Baker and co-workers in 2007.[12a] Manner's group lately employed easily available iron carbonyl complexes, $[CpFe(CO)_2]_2$ and $CpFe(CO)_2I$, activated upon UV photoirradiation. These complexes were able to catalyze the dehydrogenation of AB or Me_2NHBH_3.[12b] The bis(phosphinite) iron(II) POCOP–pincer complexes were prepared and tested for AB dehydrogenation at 60 °C leading to borazine and polyborazilene coproducts. (^{i}PrPOCOP)Fe–(H)$(PMe_2R)_2$ [R = Me or Ph; ^{i}PrPOCOP = 2,6-(iPr2PO)$_2C_6H_3$] and [2,6-(iPr$_2$PO)2-4-(MeO)C_6H_2]Fe$(PMe_2Ph)_2$ H with unprecedented activity (2.3–2.5 eq. of H_2 release per AB equivalent in 24 h at 60 °C in THF/dig).[12c] In 2015, Schneider reported a five-coordinated iron complex (PNP)eFeH(CO) [PNP = N$(CH_2CH_2PiPr_2)_2$], which release 1 eq. of H_2 with high catalytic activity and generates a linear polyaminoborane.[12d] Recently, a series of iron complexes bearing both amido and phosphine supporting ligands [e.g., Fe(DCPE)$(PhNCH_2)_2$] were synthesized by Baker, Gordon, and co-workers.[12e] They also carefully examined the catalytic activity, ammonia borane was able to release 1–1.7 equivalent of H_2 at 60 °C.

On the base of this state of the art, the development of stable molecular iron complexes for AB dehydrogenation remains highly desirable for the exploitation in industrial application. With this aim in mind a series of iron complexes bearing the combination of the noninnocent cyclopentadienone/hydroxycyclopentadienyl ligands and N-heterocyclic carbene, previously employed by our group in redox and hydrogen-borrowing catalytic applications,[13] have been prepared and tested for the first time for this ligand combination, as catalysts for the AB dehydrocoupling. The complexes analyzed in this work (**1**, **2,** and **3** in **Figure 1**) are stable and capable to overcome 1 eq. of H_2

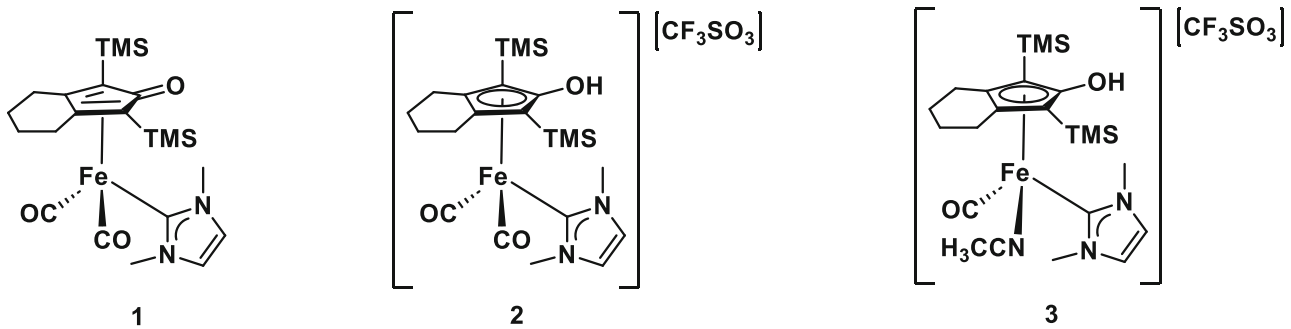

Figure 1. Iron complexes employed in this work.

Research Article
doi.org/10.1002/ejic.202500203

production. NMR characterizations allow the identification of soluble coproduct, while in situ IR experiments reveal a different mechanistic behavior comparing the neutral complex **1** and the cationic **2** and **3**. Scale-up of the reaction in a 217 mL photoreactor permits to quantify H_2 production and catalysts **1** and **2** activations, by means of CO releasing measurement.

2. Results and Discussion

2.1. Synthesis and Reactivity of Iron NHC Complexes

Iron(0) complex **1**, previously reported by the research group for the mutual role in redox properties of the cyclopentadienone, N-heterocyclic carbene ligand combination[14] can be easily protonated by a stoichiometric amount of trifluoromethanesulfonic acid leading to the corresponding iron(II) **2** complex in analogy to what is observed for similar ruthenium complexes.[15] Upon the addition of CF_3SO_3H (1 eq.) to a solution of **1** in Et_2O, precipitation occurred, yielding a light-yellow solid in quantitative yield (**Scheme 2**) The solid was identified by IR and NMR spectroscopy as the corresponding cationic iron **2** complex.

The reaction has been followed by IR analysis showing the disappearance of the cyclopentadienone C=O stretching (1568 cm^{-1}) and the concurrent strong blueshift of the CO stretching frequencies (e.g., **1**: $\upsilon(CO) = 1983$, 1922 cm^{-1} vs. **2**: 2023, 1975 cm^{-1}) (Figure S1,S2, Supporting Information) typical of the expected decrease of Ru-CO back-bonding, attributable to the cationic charge of the complex due to the formally oxidation of the metal center from Fe(0) to Fe(II). ^{13}C-NMR analysis gave further insights on the structure of the compound: coordination of the dienone ligand switching from η^4-cyclopentadienone to η^5-hydroxycyclopentadienil, consistent with the shift to higher field resonance of the ketone-enol carbon (δ $\mathbf{1}_{C=O}$: 176 ppm vs. $\mathbf{2}_{C\text{-}OH}$: 145 ppm). The Fe-NHC carbon signal is also shifted to higher-energy field ($\delta(C_{carbene})$ **1**: 184 ppm vs. **2**: 176 ppm) (Figure S3, Supporting Information).

The molecular structure of **2** has been determined by single-crystal X-ray diffraction (**Figure 2**), and supports protonation of the cyclopentadienone O(3) atom. The Fe1–C3 distance of **2** [2.118(5) Å] is considerably shorter than in the parent complex **1** [2.359(2) Å][14a] and very close to the other Fe1–C4/5/6/7 distances [2.121(4)–2.154(4) Å], suggesting a η^5-coordination of the hydroxycyclopentadienyl ligand. In keeping with the restored

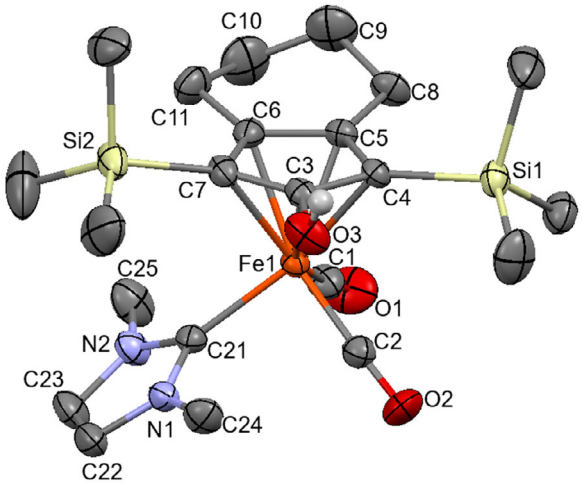

Figure 2. ORTEP drawing of **2**. Displacement ellipsoids are at the 30% probability level. Hydrogen atoms, except that bonded to O3, have been omitted for clarity. Selected bond lengths (Å): Fe1—C1 1.774(6), Fe1—C2 1.775(6), Fe1—C3 2.118(5), Fe1—C4 2.121(4), Fe1—C5 2.125(4), Fe1—C6 2.123(4), Fe1—C7 2.154(4), Fe1—C21 1.981(5), C1—O1 1.137(7), C2—O2 1.140(6), C3—O3 1.382(6), C21—N1 1.353(6), C21—N2 1.369(6), C22—C23 1.304(9), N1—C22 1.381(7), N2—C23 1.374(7), sum at C21 359.9(7), sum at C3 359.9(7), sum at N1 359.9(8), sum at N2 360.0(8).

aromaticity of the cyclopentadienyl ring, the C3–O3 contact of **2** [1.382(6) Å] is a single bond, whereas it displayed a double bond character in the parent **1** [1.250(3) Å]. Similar bonding parameters have been reported for the related [Fe(η^5-1,3-bis(trimethylsilyl)-4,5,6,7-tetrahydroinden-2-ol)$(CO)_2$ H] complex.[16] As a consequence of the reducedπ-character of the Fe–CO interactions of the cationic complex compared to the neutral one, the Fe1–C1 [1.774(6) Å] and Fe1–C2 [1.775(6) Å] contacts of **2** are slightly longer than in **1** [1.747(3) and 1.754(3) Å], whereas the opposite trend is observed for the Fe1–C21 bonding distance [1.981(5) and 1.996(3) Å for **2** and **1**, respectively]. The OH group of the cation of **2** is involved in a H-bond with the triflate anion, further supporting its location.

Upon irradiation at 365 nm of **2** in acetonitrile, the bright yellow solution turned to deep red in a few minutes. The new reddish complex **3** is an iron(II) compound with the free vacant site obtained upon CO removal, suddenly occupied by acetonitrile ligand (**Scheme 3** bottom). Activation trial by means of Me_3NO was useless due to instant deprotonation of complex **2** to complex **1** (Scheme 3 up).

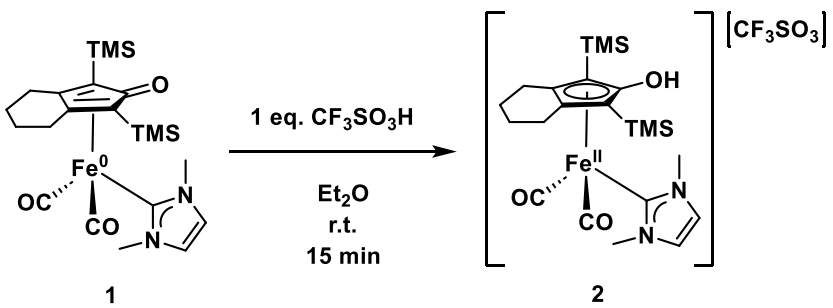

Scheme 2. Synthesis of the cationic hydroxycyclopentadienyl iron complex **2**.

Research Article
doi.org/10.1002/ejic.202500203

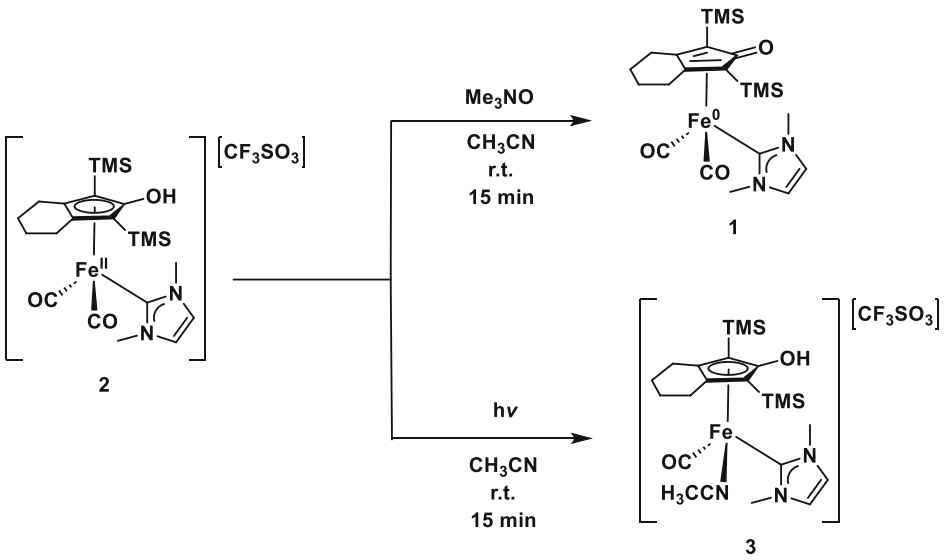

Scheme 3. Synthesis of **3** by CO removal in CH_3CN under UV irradiation (365 nm).

The reaction has been followed by IR which shows the disappearance of two CO stretching bands attributable to **2** (2023, 1973 cm^{-1}), with the concomitant appearance of a single CO band deriving from **3** (1950 cm^{-1}). Although compound **3** exhibits its slight stability in solution, it was characterized by NMR spectroscopy under an inert atmosphere. The ^{1}H and ^{13}C NMR spectra (Figure S3,S4, Supporting Information) display the typical pattern of hydroxycyclopentadienyl iron NHC complexes. However, a split in the signals is observed, likely due to the replacement of one CO ligand with acetonitrile, resulting in a lower symmetry structure. Carbene resonance shifts downfield, from 169.6 (**2**) to 179.9 ppm (**3**) because of the difference electronic environment due to the presence of a relatively weak σ-donor and a poor π-acceptor compared to CO. Unless what observed for **2**, which is stable to air and moisture for months if kept in the dark, the species **3** is stable only a few minutes at air in acetonitrile solution and must be handled under an inert atmosphere.

2.2. AB Dehydrocoupling

Iron complexes **1** and **2** were evaluated as catalyst precursors for AB dehydrocoupling following the reaction by NMR. Treatment of NH_3BH_3 (AB) solution in THF with **1** and **2** (10 mol% Fe) at room temperature for 2 h in a closed vessel system (a J-young NMR tube) led to poor formation of trimer B-(cyclodiborazanyl) amine-borane (BCDB), as indicated by ^{11}B-NMR spectroscopy. At about −43 ppm a quintuplet was clearly visible with a $J_{B\text{-}H} = 80$ Hz, which is typical of borohydride (BH_4^-) anion.[11a] Upon warming up at 60 °C for 24 h, a significant conversion was detected for both complexes (81% for **1** and 82% for **2**), although to a detriment of selectivity: insoluble polymer was visible in the mixture and BCDB and borazine were detected by ^{11}B-NMR.

Since the cationic Fe(II) species **2** undergoes easily CO releasing upon photoirradiation, a solution of AB in THF containing 10 mol% of **2** was irradiated with a common Hg lamp (125 W). Molecular H_2 evolution was visible, by bubble formation in the NMR tube (for H_2 quantification, vide infra), after a few seconds a complete conversion was detected in about 50 min (**Figure 3**). Analysis of reaction mixture with ^{11}B-NMR revealed a mixture of trimer cyclotriborazane (CTB, ^{11}B-NMR: $\delta = -12.0$ ppm), polymer (broad at ^{11}B-NMR: $\delta = -5.6$ ppm), and borazine (^{11}B-NMR: $\delta = 30.9$ ppm).[11a] After a night at room temperature without irradiation, all CTB disappeared, likely converted to borazine and further dehydrogenated to polyborazylenes (broad ^{11}B-NMR: $\delta = 31.2$–26.1 ppm). At about $\delta = -37.1$ ppm (^{11}B-NMR) a quartet ($J_{B\text{-}H} = 86$ Hz) was detectable throughout all experiments, and it was assigned to carbene–BH_3 complex, as comparable to literature values,[17,18] showing a partial decomposition of **2**.

In order to shed some light on selectivity of the reaction, a test was performed in an open vessel under nitrogen atmosphere. Irradiation of the solution led to a complete conversion of AB and after 4 h no boron species were detected by ^{11}B-NMR spectroscopy in solution (**Figure 4**). Unlike the closed vessel reaction, formation of borazine was not concurrent to polyaminoboranes formation (no broad signals around ^{11}B-NMR: $\delta = -5.6$ ppm); indeed, borazine is a volatile liquid (bp 53 °C) and an open vessel setting might shift the equilibrium to the borazine as final product. As for the closed vessel, the quartet at $\delta = -37.1$ ppm (^{11}B-NMR) assigned to NHC-BH_3 was clearly visible throughout all reaction time.

The corresponding neutral complex **1** was also evaluated as photocatalyst. Irradiating a solution of AB in THF led to poor reactivity compared to the cationic **2**. Indeed, AB reagent was still detected together with a mixture of BCDB, insoluble polyaminoboranes, and borazine after 4 h.

Due to the good results with **2** under photocatalytical conditions, the acetonitrile-substituted Fe(II) derivative **3** was evaluated as precatalyst in order to avoid any preactivations (thermal or irradiation) of the reaction mixture. Indeed, treatment of AB solution in THF with **3** (10 mol% at room temperature) led to instantaneous H_2 evolution with formation of insoluble polyaminoboranes. Complete conversion was achieved after stirring for 4 h (**Figure 5**). No signals were detected at ^{11}B-NMR of

Research Article
doi.org/10.1002/ejic.202500203

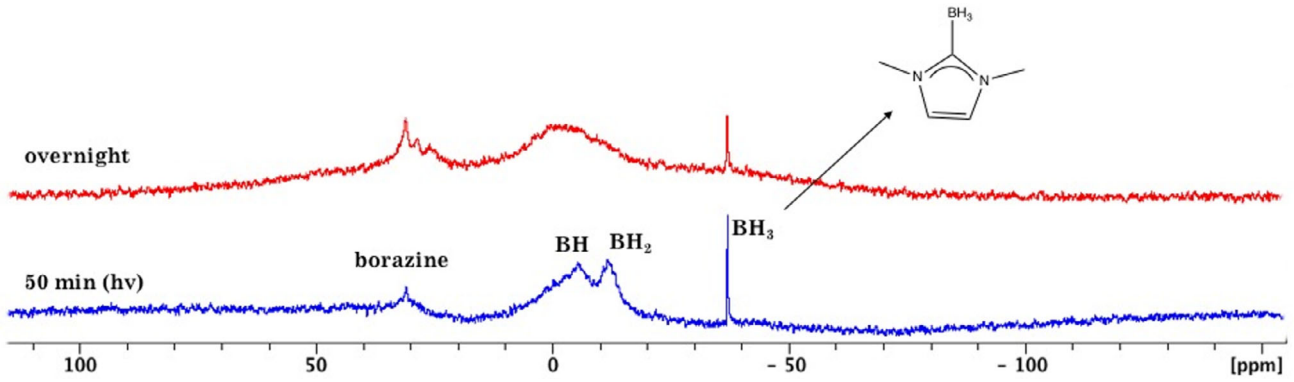

Figure 3. $^{11}B\{^1H\}$-NMR spectrum (THF) showing the reaction crude upon reactivity of **2** after 50 min of irradiation (blue) and after stirring overnight at room temperature (red).

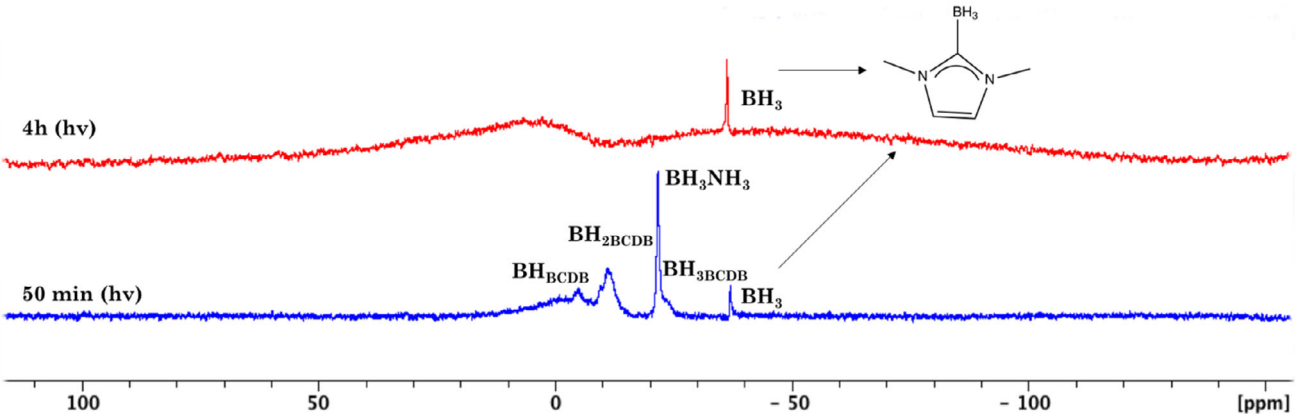

Figure 4. $^{11}B\{^1H\}$-NMR spectrum (THF) showing the reaction mixture with **2** in open vessel after 50 min of irradiation (blue) and after 4 h (red).

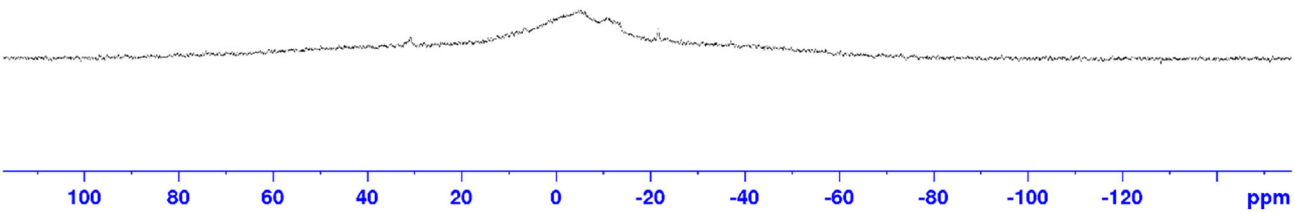

Figure 5. $^{11}B\{^1H\}$-NMR spectrum (in THF) showing the reaction mixture with **3** after 2 h. No soluble B compounds were detected.

NHC-BH_3 species at about $\delta = -37.1$ ppm, suggesting that very mild conditions avoid decomposition of the iron complex due to NHC detachment. ^{1}H-NMR showed a low signal of a hydride (^{1}H-NMR: s, $\delta = -13.9$ ppm), likely a resting state of the catalyst. **3** performed quantitative conversion down to 2 mol% of catalyst loading. Furthermore, **3** showed high selectivity in polyaminoboranes; hence, it can be classified as Type I catalyst, which releases up to one equivalent of H_2 per equivalent of AB.

2.3. Mechanistic Investigation

Once defined preliminary information from NMR tube reactions, catalytic activity studies have been moved to a 217 mL photoreactor (Figure S10, Supporting Information) to monitor catalyst's activation behavior by quantitative measurement of CO released by the precatalyst. Further information on the catalyst and substrate role in the reaction has been collected with a peculiar in situ IR technique that includes a system designed to allow the gas evolution from the IR cell while keeping the measured mixture homogeneous.

2.4. Catalyst 1 and 2: Activation Studies

In order to quantitatively follow the CO release from the catalyst by means of gas chromatography (GC) measurements, the reaction has been at first studied with a substantial precatalyst ratio of 25 mol%.

Research Article
doi.org/10.1002/ejic.202500203

The two complexes, neutral **1** and cationic **2** (0.027 mmol), were activated by irradiation in a 217 mL photoreactor at room temperature, in 50 mL of anhydrous THF in the presence of 1.1 mmol of substrate. Once the reactor was purged with nitrogen at atmospheric pressure the first headspace sampling has been carried out, before irradiating. White light emitting diode (LED) light has been then switched on. The reaction was followed by sampling the headspace every 5 min.

The measurement of CO released from precatalysts **1** and **2** as a function of time is depicted in **Figure 6**. Interestingly, CO releasing rate is similar for the neutral **1** and the cationic complex **2** in the first 25 min of the reaction. Lately while **1** keep losing CO, the cationic counterpart shows a decrease due to the withdrawals, demonstrating that the neutral catalyst **1** reach a higher degree of activation (18%) than **2** (14%). This behavior is quite peculiar if we consider the Ru–CO back bonding, which would be higher in the case of **1** rather than **2**. In fact, blank experiments show the photoremoval of a CO ligand from **2** in THF leading to the increase of a new band at 1920 cm^{-1}, in the absence of substrate (Figure S11, Supporting Information), but demonstrated that neutral complex **1** is stable under the same conditions (Figure S12, Supporting Information). Thus, the activation of **1** under AB dehydrogenation conditions looks to be ascribable to an interaction between the substrate and catalyst **1**.[19] In principle, a hydrogen bond with cyclopentadienone C═O oxygen, which is known to reduce the electron density on the metal, could be reasonably involved in the activation, as in similar ruthenium-based precatalysts.

Hydrogen productivity in mol/min is plotted together with the turn over frequency (TOF) (s^{-1}) values versus time in **Figure 7**, confirming a lower activity for the neutral complex **1** compared with the cationic one **2** (e.g., 1.47 mol H_2/mol AB for **2** vs. 0.34 mol H_2/mol AB for **1** at 50 min; 2.08 mol H_2/mol AB for **2** vs. 0.57 mol H_2/mol AB for **1** at 70 min). TOF numbers

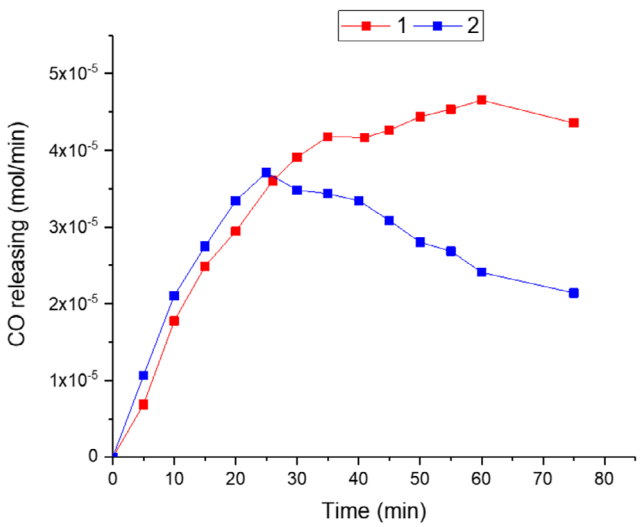

Figure 6. CO releasing quantification (mol/min). Reaction conditions: THF (50 mL), AB (1,1 mmol), catalyst loading (25 mol%). Catalyst **1** red line, catalyst **2** Blue line.

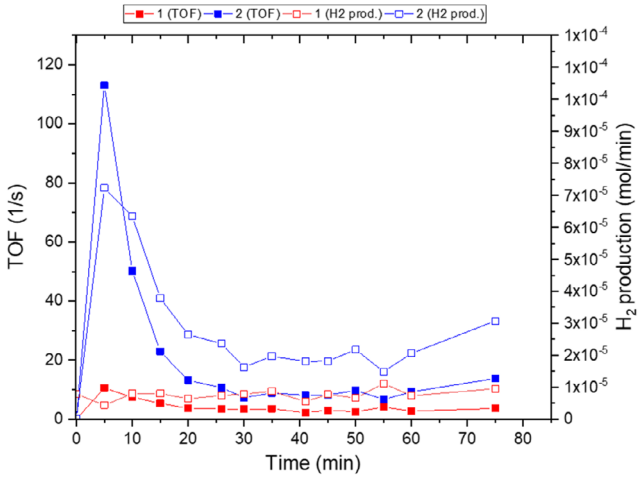

Figure 7. Hydrogen productivity (mol/min) and TOF behavior (1/s). Reaction conditions: THF (50 mL), AB (1,1 mmol), catalyst loading (25 mol%). Catalyst **1** red line, catalyst **2** Blue line. Full symbols are related to TOF, empty symbols to hydrogen productivity.

reported in Figure 7 were calculated using the real amount of activated catalyst reported above.

More in general H_2 evolution reaches (blue line) a maximum at 5 min (7.32×10^{-5} mol min^{-1}, ≈113 s^{-1} TOF) for the cationic species **2 and** then decreases to 2×10^{-5} mol min^{-1} in 20 min. On the other hand, productivity for precatalyst **1** is lower (4.37×10^{-6} mol min^{-1}, ca. ≈10 s^{-1} TOF), but stable since the beginning of the reaction.

By lowering the catalyst loading to 5 mol%, a similar behavior in terms of activation of catalysts **1** and **2** is obtained. As reported in **Figure** 1 and **8,** CO is lost somewhat slowly reaching a maximum activation of 20% of the precatalyst; on the other hand, **2** shows a faster removal of CO reaching a 32% activation of the cationic precatalyst.

It is interesting to note that while precatalyst **1** maintains a ≈20% activation both in the case of 25 and 5 mol% catalyst loading, precatalyst **2** reaches in the latter case, a sensitive higher relative rate of activation (from 14% to 32%). This difference could be again ascribed to the fact that activation of **1** involves a role of the substrate. Nevertheless, as it can be expected, the absolute quantity of CO release is lower at 5 mol% also for **2**.

More in general in the case of lower catalyst loading, the initial activation rate of **2** is faster than for **1**, highlighting that the activation rate of **1** is influenced by the amount of catalyst. However, in line with the behavior with a 25 mol% loading, **2** shows a sensitive reduction in CO release after a rapid activation. On the opposite **1** suffers an induction period, but preserves a constant behavior for a longer time.

Figure 9 shows TOF trend and hydrogen production with 5 mol% of catalyst loading. As in the 25 mol% case **1** is slower than **2** in the early stage of activation. Lately, while catalyst **1** shows a slight decrease in TOF along the reaction, catalysts **2** speed is quite stable (opposite to the 25 mol% behavior), suggesting a kinetic trend of the cationic active species **2** likely dependent on the available substrate in its original form (AB

Research Article
doi.org/10.1002/ejic.202500203

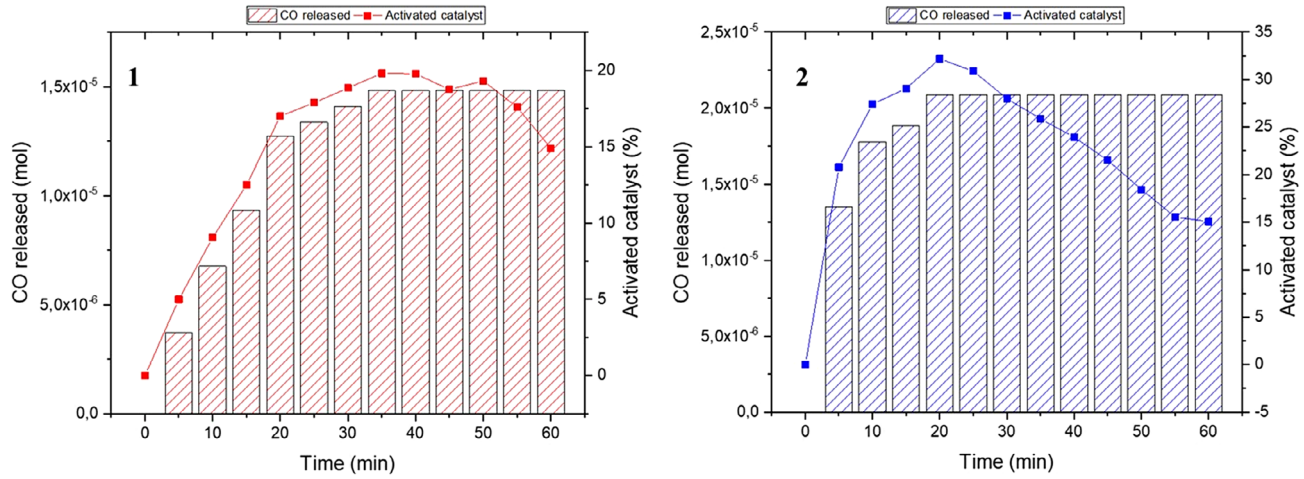

Figure 8. CO releasing quantification (line) and % catalyst activated (bars) versus time. Reaction conditions: THF (50 mL), AB (1,1 mmol), catalyst loading (5 mol%). Catalyst **1** left, catalyst **2** right.

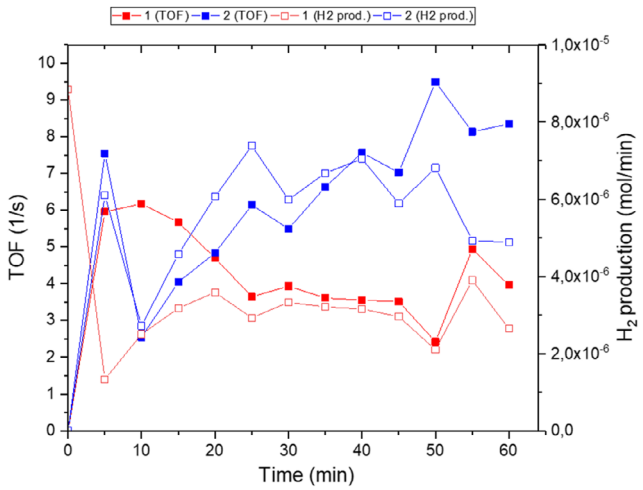

Figure 9. Hydrogen productivity (mol/min) and TOF behavior (1/s). Reaction conditions: THF (50 mL), AB (1,1 mmol), catalyst loading (5 mol%). Catalyst **1** red line, catalyst **2** Blue line. Full symbols are related to TOF, empty symbols to hydrogen productivity.

before the first equivalent dehydrogenation). Indeed, hydrogen productivity, measured at 50 min (5 mol%: 0.27 mol H_2/mol AB for **2** vs. 0.16 mol H_2/mol AB for **1**; 25 mol%: 1.47 mol H_2/mol AB for **2** vs. 0.34 mol H_2/mol AB for **1**), shows the complete consumption of AB (hydrogen productivity >1) in the case of **2** at 25 mol%, followed by a decrease in TOF value after 20 min, which is not observed in the case of 5 mol% (hydrogen productivity <1). In general, catalyst **2** is further confirmed as the more active one. Although working at room temperature with low to interesting productivity, our catalysts do not reach the best properties of iron catalyst reported up to date. Nevertheless, the novel ligand combination and the slow reactivity candidate **1**–**3** are to be studied from a mechanistic point of view both from the AB and the catalyst side, for a future plan to better design ligands substituents in order to improve activity.

Indeed, further evidence of the influence of the substrate can be found monitoring the role of reaction concentration (0.02 M in 50 mL; 0.06 M in 20 mL; 0.1 M in 10 mL). In **Figure 10** it is interesting to note that catalyst **1** speed is generally negatively affected by increased concentration (red and pink lines, 50 mL, 10 mL), while speed of **1** at initial time seems to be only smoothly affected by solvent volume. Nevertheless, catalyst **2** has indeed a boost in the initial reaction activation while decreasing the reaction volume (blue, light blue lines 50 mL, 10 mL). In order to have an intermediate data, for catalyst **2** the experiment was also conducted at 20 mL (mid blue line), confirming that the behavior is related to concentration.

Hydrogen productivity at 50 min, expressed in terms of equivalents (mol H_2/mol AB) versus THF volume, is reported in **Table 1**.

The detrimental effect on catalyst **1** of the increased concentration is also confirmed by productivity, measured as H_2 produced in 50 min (entry 1, 0, 13 eq. in 50 mL vs. entry 2, 0.05 eq. in 10 mL). Conversely, CO release, which would likely influence catalyst activation, improves at higher concentration

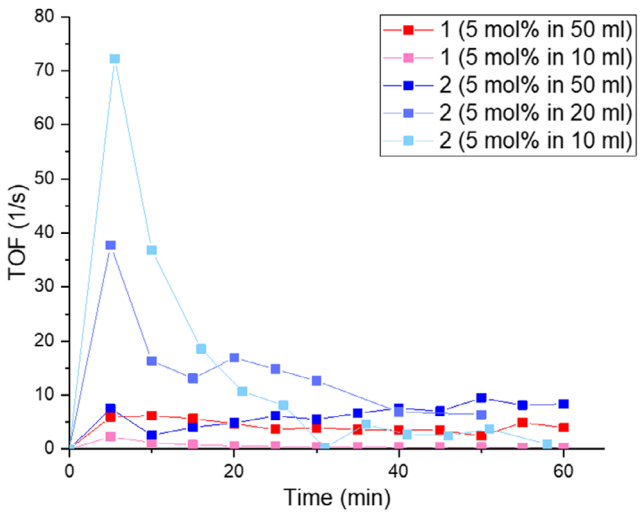

Figure 10. TOF behavior (1/s) versus time at different concentrations. Reaction conditions: AB (1,1 mmol), catalyst loading (5 mol%). Catalyst **1**: red and pink lines, catalyst **2**: Blue, mid blue, light blue lines.

Research Article
doi.org/10.1002/ejic.202500203

Table 1. Hydrogen equivalents produced and percentage of active catalyst (calculated from CO release measurement) for catalysts **1** and **2** varying the solvent volume. Conditions: AB (1,1 mmol), catalyst loading (5 mol%), 50 min.

Entry	Catalyst	THF (mL)	mol H_2/mol AB (eq.)	active catalyst (%)*
1	**1**	50	0.13	19
2	**1**	10	0.05	63
3	**2**	50	0.27	32
4	**2**	20	0.27	14
5	**2**	10	0.25	15

(19% in 50 mL vs 63% in 10 mL). Although this latter finding can be explained taking into account the proposed role of AB in promoting the CO release from neutral complex **1** (which would be more effective at higher concentration), the countertrend efficiency opens some questions on the active species and/or stability of the catalyst over concentration variation.

Efficiency for catalyst **2** at 50 min appears to be similar at different concentrations [entry 3–5: 0.27 (50 mL), 0.27 (20 mL), and 0.25 (10 mL)], although catalyst activation measured by CO release is higher at lower concentration (entry 3–5 32% in 50 mL, 14% in 20 mL, and 15% in 10 mL). This agrees well with TOF behavior in Figure 7 which is more favored in the short time for higher concentration and in the long time for lower concentration.

Catalysts efficiency verses time at 5 mol% was also checked at 240 min in 50 mL (80 min: 0.32 eq. for **1** and 0.45 eq for **2**). Both the catalysts result to be active at higher times.

Finally, to evaluate the activity of the resting state, a fresh dose of 1.1 mmol of AB was added to the crude mixture in in THF (20 mL).

With the aim of confirming the role of CO release in the catalyst activation and to better understand the catalyst stability, the preactivated form of the cationic catalyst **3** was employed under the photoreactor conditions. Complex **3** synthetized in THF under N_2 atmosphere is then transferred to the photoreactor keeping it in inert conditions. The substrate is then added to have a catalytic load of 5 mol%. The results in terms of TOF and hydrogen production per minute are shown in **Figure 11**.

Interestingly, both the catalyst's productivity and TOF value have their maximum at the very beginning of the reaction. Comparing the graph of **3** with that of **2** in Figure 9 we can observe a parallel behavior with a delay, in the latter case, ascribable to the induction time due to the activation. This definitively confirms that the active form of the catalyst has to follow the CO release.

However, it is also important to underline that the instant catalytic activity is accompanied by a rapid deactivation in 15 min.

2.5. Analysis of the Insoluble Coproducts

To characterize the coproducts obtained performing the reaction in photoreactor, the precipitate was recovered by filtration and analyzed by XRD (Figure S13, Supporting Information) after drying at room temperature in air. In both the cases **1** and **2**, the solid

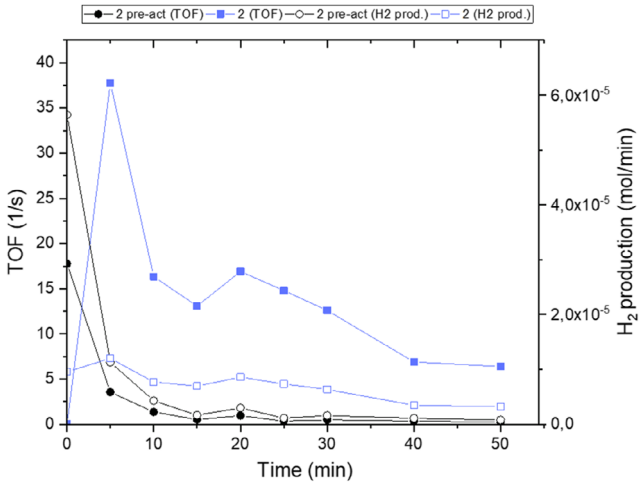

Figure 11. Hydrogen productivity (mol/min) and TOF behavior (1/s). Reaction conditions: THF (50 mL), AB (1,1 mmol), catalyst loading (5 mol%). Preactivated catalyst **3**: black line; catalyst **2**: Blue line. Full symbols are related to TOF, empty symbols to hydrogen productivity.

corresponds to the crystalline form of ammonium tetrahydroxohesaoxotetraborate dihydrate (ref. code: 98-005-6864). The dehydrogenated form of AB (e.g., polyaminoborane oligomers) undergoes to oxidation and hydrolysis when exposed to the atmosphere producing the abovementioned structure as previously reported.[20]

2.6. In Situ IR Characterization

As previously demonstrated catalyst **1** and **2** are expected to behave in different catalytic mechanisms. To investigate the catalysts activation and interaction with the substrate AB, the reaction was followed by in situ IR technique consisting of a infrared fourier transform (FTIR) cell equipped with an injection system and a purge for the elimination of the gasses produced during the reaction (Figure S14, Supporting Information). The cell was continuously irradiated during the reaction time.

2.7. Reactivity of Catalyst 1

A blank test was conducted by monitoring the evolution of a THF substrate solution during irradiation in order to verify the stability of AB under reaction conditions (Figure S15, Supporting Information). The spectra, which show the AB stretching at 3310, 3239, 3180 and 2361, 2319, 2275, 2213 cm^{-1} for the NH_3 and BH_3 moiety, respectively,[21] did not change during reaction time, demonstrating the stability of the substrate in THF under irradiation. Then, AB was reacted, under photolytic dehydrogenation conditions, with a stoichiometric amount of the neutral catalyst **1** in anhydrous THF. As depicted in Figure 10, analyzing the AB region of the IR spectrum, it is reasonable to confirm that the substrate could be involved in the catalyst activation. In **Figure 12**, the spectra recorded as the difference with the black spectrum registered before irradiation show the growth of two bands at 3491 and 2450 cm^{-1}, which is likely to arise from an

Research Article
doi.org/10.1002/ejic.202500203

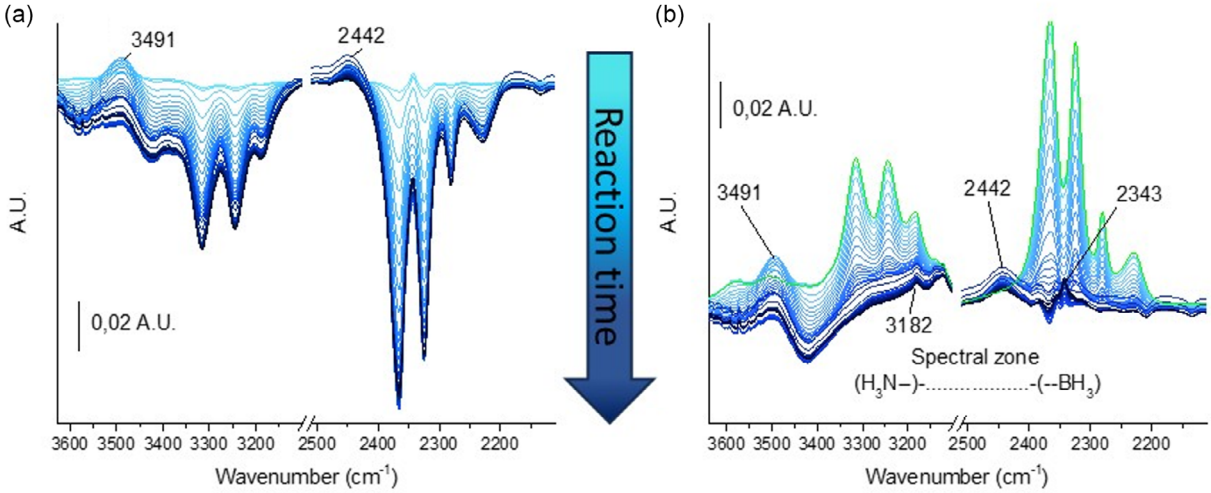

Figure 12. Evolution of AB under dehydrogenation reaction in presence of stoichiometric amount of **1**: a) spectra obtained by difference with the spectrum registered before irradiation; b) spectra obtained by difference with the THF spectrum.

intermediate resulting from the interaction between catalyst **1** and the substrate, probably ascribed to borazine moiety.[22] Lately, AB spectrum further evolve to the final form characterized by two bands at 3182 and 2343 cm^{-1} (Figure 12b).

The two final bands at 3182 and 2343 cm^{-1} are not ascribable to neither borazine,[23] nor BH_4[24] species.

However, it is possible to hypothesize that the latter two bands are ascribable to polymeric amminoborane $(H_2BNH_2)_n$ or $(HNBH)_n$.[25] By comparison with NMR characterization discussed above, we expect the same soluble compounds observed under **1** catalytic condition (i.e., BCDB and/or soluble polyborazine).

Analyzing the same spectra evolution in the region of CO stretching frequencies of **1** (**Figure 13**) we can observe two shoulders arising at higher wave numbers (1999, 1942 cm^{-1}) with respect to the precatalyst symmetrical and antisymmetric CO stretching (1984 and 1923 cm^{-1}) before the irradiation. These can be thus attributable to the **1**/AB adduct which allows the CO release. The AB interaction with **1** decreases the back bonding of the metal center to the terminal CO, thus proving to be the promoter for the UV-mediated cleavage of Fe—CO bond in **1**. Then, as soon as the irradiation is switched on, the growth of a band at 1879 cm^{-1}, ascribable to a mono carbonyl catalytic species, is detected.

Soon after, another band of a monocarbonyl species at 1894 cm^{-1} starts to grow at higher wave number, also reaching a maximum when starting AB is still present in the reaction medium. This new bands could fit with the formation of two hydride complexes Fe–H (band at 2066 and 2043 cm^{-1}),[26] one that is expected to be formed from the concerted dehydrogenation of AB (1a in **Figure 14**) and the second, if associated to the bands in the –BH and –NH region 3491 and 2450 cm^{-1}, that can arise from the formation of the intermediate proposed for a similar reactivity with the ruthenium Shvo complex (1b in Figure 14)[27] which is expected to show IR band in this region[23] and which has been identified as a responsible for the low activity

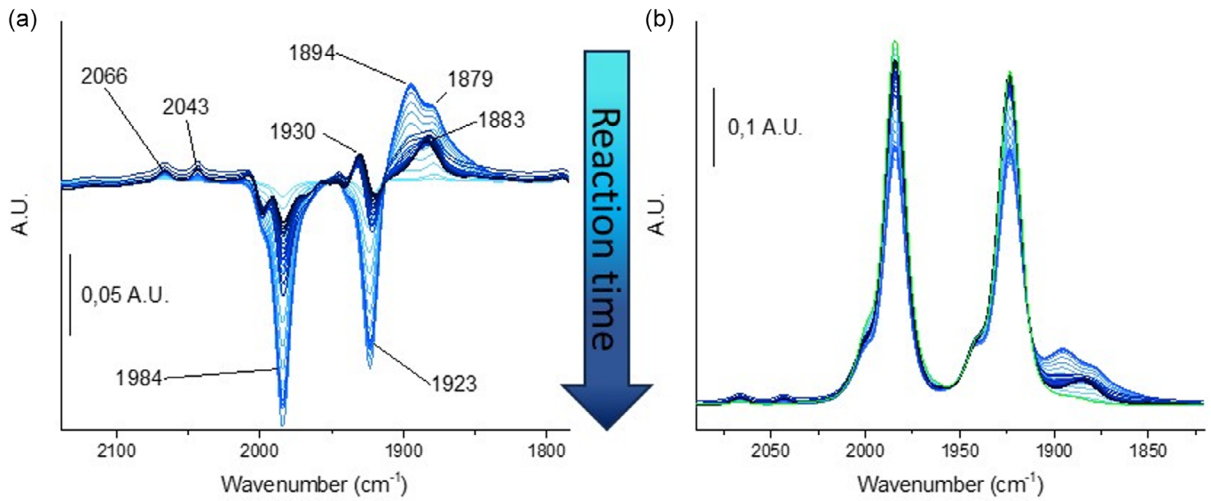

Figure 13. Evolution of CO under dehydrogenation reaction in presence of stoichiometric amount of catalyst **1**: a) spectra obtained by difference with the spectrum registered before irradiation; b) spectra obtained by difference with the THF spectrum.

Research Article
doi.org/10.1002/ejic.202500203

Chemistry Europe
European Chemical Societies Publishing

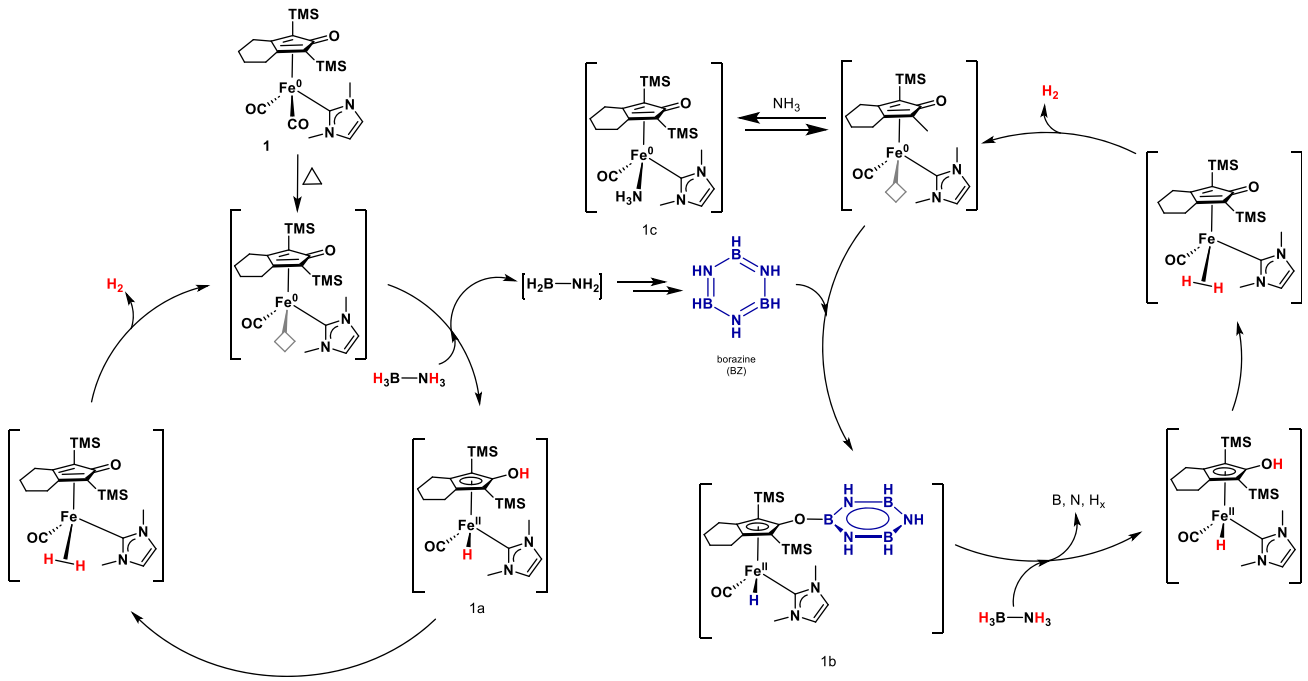

Figure 14. Proposed mechanism of complex 1 acting as a catalyst in the dehydrogenation reaction of aminoboranes (ABs).

of the ruthenium complex in AB dehydrogenation as well. Interestingly, once AB is completely converted, the two bands (1879 and 1894 cm^{-1}) rapidly decrease converging in a new weak band at 1883 cm^{-1}. We can consider it a resting state, again probably suffering from the same deactivation mode of Shvo complex due to NH_3 coordination (1c in Figure 14). Indeed, the catalyst, as described above (productivity < 1 mol H_2/mol AB in all the cases), looks to be not active anymore for a further dehydrogenation.

2.8. Reactivity of Catalyst 2

Blank irradiation of the cationic hydroxycyclopentadienyl NHC iron complex **2** in THF confirms that in this case the interaction with the substrate is not involved in the CO release. Indeed, IR bands of **2** at 2023 and 1970 cm^{-1} eroded, while a new band at 1922 cm^{-1} attributable to a derived complex with a single band in the CO region grows up (Figure S11, Supporting Information).

In **Figure 15** the spectra obtained by monitoring the AB dehydrogenation using stoichiometric amount of catalyst **2** is reported.

AB spectra along with reaction time follows a different pathway in the case of **2**. Intermediates show different bands in the -NH and -BH region (3110 and 2450 cm^{-1}). Interestingly, at the end of the monitored period, the complete disappearance of all the bands related to AB and the formation of two bands at 3182 and 2343 cm^{-1} respectively is detected, the same is observed at the end of the reaction with **1**, further confirming

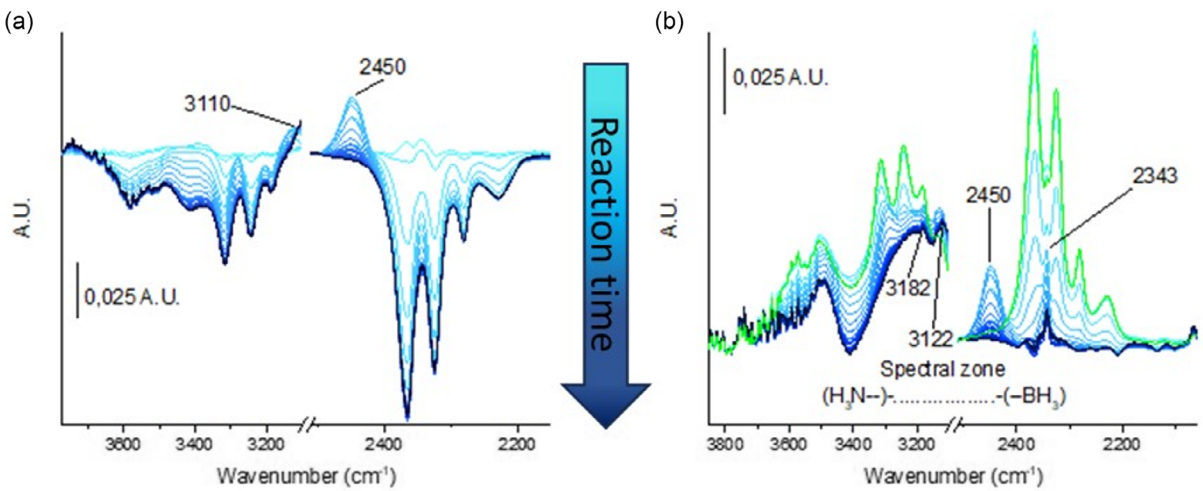

Figure 15. Evolution of AB under dehydrogenation reaction in presence of stoichiometric amount of catalyst **2**: a) spectra obtained by difference with the spectrum registered before irradiation; b) spectra obtained by difference with the THF spectrum.

Research Article
doi.org/10.1002/ejic.202500203

that these bands belong to the stretching modes ascribable to dehydroboration products, as already suggested by ^{11}B NMR characterization (Figure 3–5).

Analyzing the CO region, stretching from the precatalyst **2** (2023 and 1970 cm^{-1}) decrease during the irradiation, with an interesting parallel behavior which bring to the formation of a couple of strong bands at 1986 and 1922 cm^{-1}. The two latter bands could be attributed to the symmetric and antisymmetric CO stretching modes of **1** that are likely to be formed by deprotonation promoted by AB intermediates. The formation of **1** is also proved by the growth of the band at 1598 cm^{-1} attributable to the Cp═O stretching mode (**Figure 16**). The presence of **1** in solution from the beginning of the reaction is also confirmed by the appearing of the bands of monocarbonylic species at 1894 and 1879 cm^{-1} typical of the neutral **1** behavior (Figure 13).

Although the activated form in which we expect THF coordinated to the iron center in **2** (Figure S11, Supporting Information) cannot be visible at 1922 cm^{-1} because it is overlapped with the CO signal of **1**, two novel bands are detected at 1874 and 1850 cm^{-1}. Anyway, the latter occur at the end of the reaction and are, therefore, more likely attributable to the resting state rather than to the intermediates. Due to the superimposition of the spectra arising from **1** and **2**, we can only observe that the cationic catalyst **2** is likely to work in favor of the activation.

Same characterization on the preactivated complex **3** obtained in acetonitrile and followed by IR with a shift of the bands from 2026 and 1976 cm^{-1} (**2**) to 1950 cm^{-1} (**3**) (Figure S16, Supporting Information) was recorded after drying the monocarbonylated **3**, dissolving it in anhydrous THF and adding a stoichiometric amount of substrate (**Figure 17**).

From Figure 17 (left) it is possible to verify that the substrate undergoes to complete conversion. During the dehydrogenation process the same band detected for **2** in the –BH region is observed at 2450 cm^{-1}. This disappears along the reaction time. The absence of –BH and –NH stretching at the end of the reaction is likely due to precipitation of insoluble AB-derived polymers. Focusing on the carbonyl region of the iron catalyst **3** (Figure 17 - right) we can observe the replacement of the acetonitrile ligand (1942 cm^{-1}) with a THF (1922 cm^{-1}) which increases at the end of the reaction. During the reactivity two bands attributable to intermediates show up at 1889 cm^{-1} and at 1862 cm^{-1} and disappear at the end of the reaction giving rise to **3**/THF (1922 cm^{-1}). These bands are likely to be related to the 2450 cm^{-1} stretching of –BH mode. Nevertheless, this experiment, avoiding the formation of the neutral dicarbonyl species, allows to define that cationic species **2** and **3** follow a different mechanism than **1**.

With the aim to avoid deprotonation an N-substituted AB substrate has been employed for $(CH_3)_2HN\text{-}BH_3$. Results are reported in **Figure 18**. Replacing $–NH_3$ moiety with $–(CH_3)_2HN$ also simplifies the –NH region of the spectra, which present only one band due to the N–H stretching at 3210 cm^{-1} (Figure 18a).

As expected, **1** behaves, in the CO region (Figure 18b) as in the corresponding AB reactivity and deprotonation of **2** (Figure 18d) is almost completely suppressed. Indeed, it behaves as in the case of preactivated catalyst **3** (Figure 17). For **1** in the –BH, –NH, –OH region (Figure 18a), it is interesting to note that a weak band arises in the –BH region at 2450 cm^{-1}. On the other hand, a new band shows up at 3366 cm^{-1}, which is likely to be ascribable to the –OH stretching of **1b** intermediate (Figure 14) superimposed to and –NH stretching of a still unknown intermediate. In the corresponding CO region two-band growth at 1894 and 1879 cm^{-1}, hydride species are identified at 2060 and 2038 cm^{-1} as in case of use of unsubstituted AB as substrate (Figure 18b). For **2**: Concerning the –BH region (Figure 18c), the expected band is observed at 2445 cm^{-1}, while a new band at 3387 cm^{-1} in the –NH and –OH region stretching, with a trivial attribution, appears. In the corresponding CO region, an intense band at 1920 cm^{-1} that is mostly due to the monocarbonylated cationic species in solution and a pair of bands at 1889 and 1874 cm^{-1} due to the shift of CO stretching by interaction of monocarbonylated species with substrate are observed (Figure 18d).

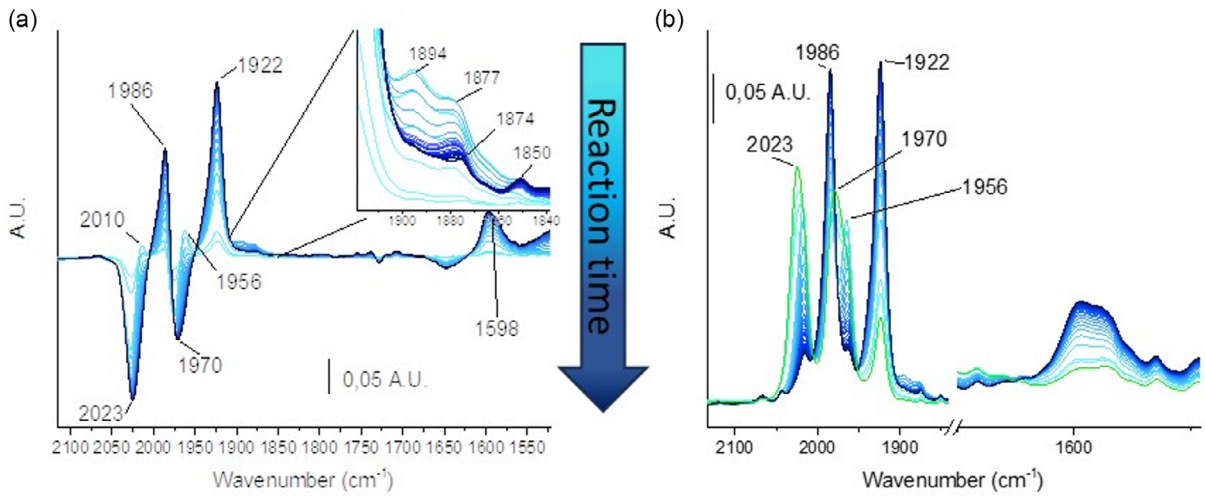

Figure 16. Evolution of CO under dehydrogenation reaction in presence of stoichiometric amount of catalyst **2**: a) spectra obtained by difference with the spectrum registered before irradiation; b) spectra obtained by difference with the THF spectrum. For justification of the band at 2010 and 1956 cm^{-1} see the supporting information.

Research Article
doi.org/10.1002/ejic.202500203

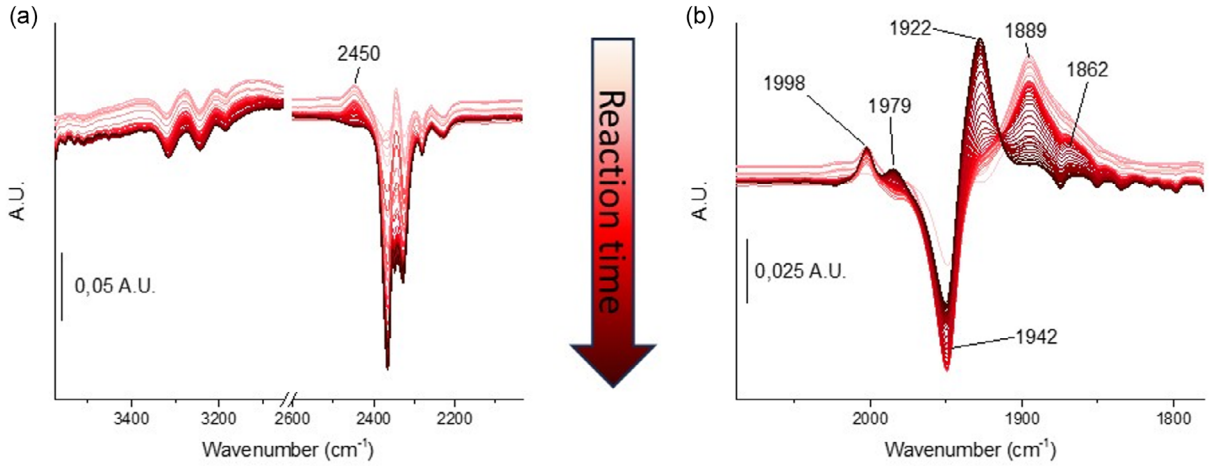

Figure 17. Evolution of AB (left) and terminal CO on the catalyst (right) under dehydrogenation reaction in presence of stoichiometric amount catalyst **3**: a) spectra obtained by difference with the spectrum registered before irradiation; b) spectra obtained by difference with the THF spectrum.

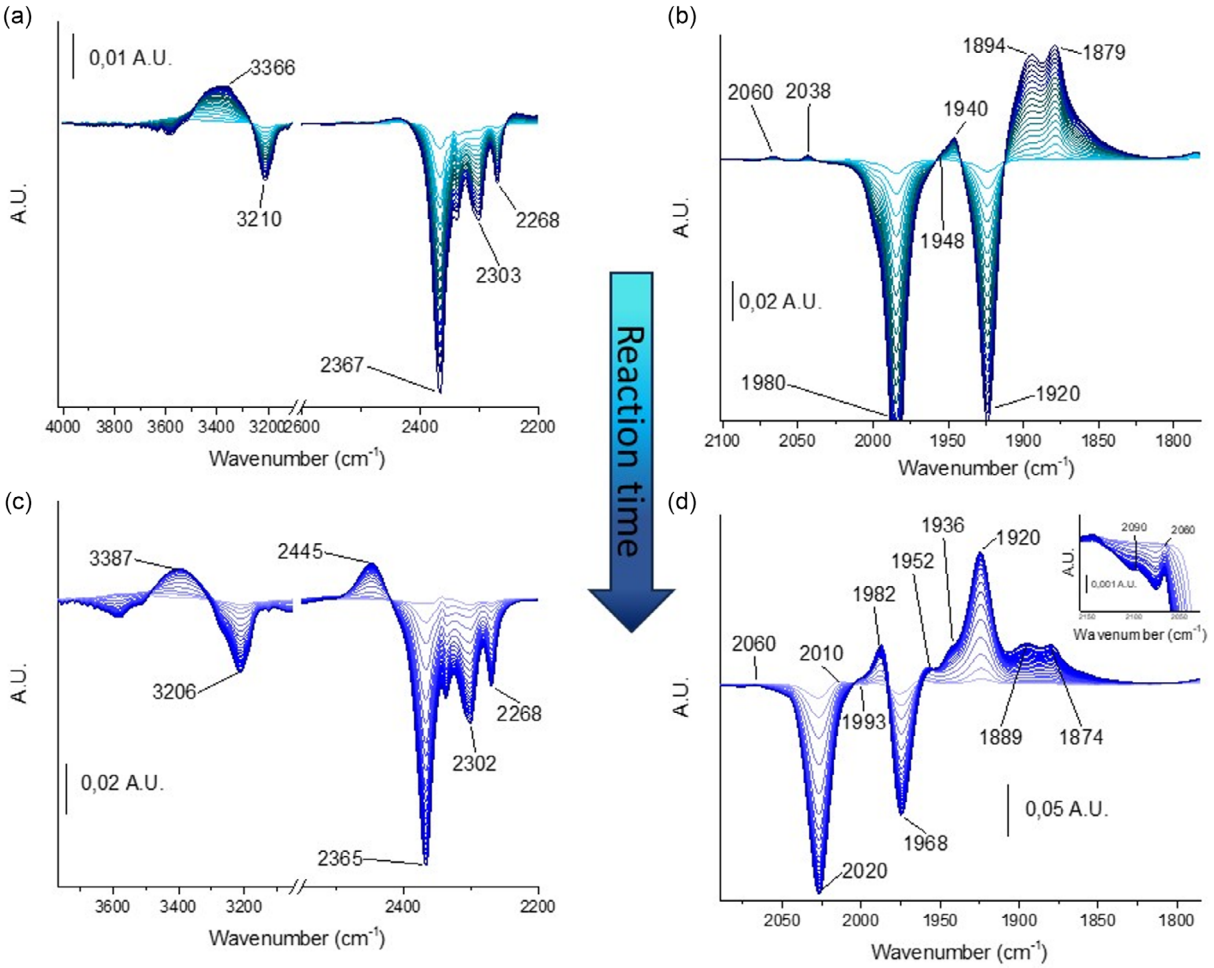

Figure 18. Evolution of AB region and terminal CO region under dehydrogenation reaction in presence of an excess of $(CH_3)_2HN\text{-}BH_3$: a,b) spectra obtained by difference with the spectrum registered before irradiation for **1**; c,d) spectra obtained by difference with the spectrum registered before irradiation for **2**.

Research Article
doi.org/10.1002/ejic.202500203

3. Conclusions

Three iron complexes based on the combination of N-heterocyclic carbene and cyclopentadienone/hydroxycyclopentadienyl ligands **1–3** have been shown to be homogeneous catalysts for AB dehydrocoupling. Precatalyst **1** and **2** are stable and need photoactivation by means of UV irradiation. The former **1** is only activated in interaction with substrate, while the cationic form undergoes activation also without AB, both in THF and in ACN. However, both release CO under catalytic conditions UV irradiation, leaving dormant the great part of the catalyst. Although **1** and **2** undergoes to a similar grade of activation, catalyst **1** is less active.

NMR experiments demonstrated that photoirradiation of **2** is selective in formation of soluble BCDB followed by borazine as end-product. Drawbacks are the need of photoactivation, borazine as end-product, since it is a well-known poison for fuel cells due to its volatility and decomposition of the catalyst by releasing of NHC.

Treatment of AB solution with the acetonitrile-substituted derivative **3** led to complete conversion in under very mild condition, avoiding irradiation of solution resulted in no decomposition of iron complex by NHC decoordination (no NHC-BH_3 evidence by ^{11}B-NMR). Furthermore, **3** performed complete conversion with a loading as low as 2 mol%.

From in situ IR characterization catalyst **1** is likely to follow a similar behavior as the one reported for the ruthenium-based Shvo catalyst, leading to deactivated intermediate and off-cycle species (due to interaction with borazine and NH_3) which slow the catalytic process. Unexpectedly, precatalyst **2** under irradiation in the presence of the substrate is partially deprotonated to **1**, thus showing a mixture of spectra of **1** and **2** as the catalytic cycle behavior. Studies of in situ IR of precatalysts **2** and preactivated catalyst **3** behavior finally allowed to identify a different band arising from **2** and **3** if compared with **1**. Indeed, the cationic species **2** and **3** show the formation of different intermediate with AB substrate, justifying the different catalytic activity. In order to further evidence the interdependent behavior of **2** and **3** reactivity of **2** has been analyzed with a substituted substrate $(CH_3)_2$N-BH_3 actually showing in the CO region the same behavior as in the case of **2** with AB substrate. The combination of scale up and spectroscopic tools, the detailed description of the catalyst activation, H_2 evolution, and role of the substrate in activation and catalytic behavior pave the way for the design of new catalyst with the aim of better exploit the electronic tuning suitable with this ligand combination and in order to improve efficiency of the whole scaled up system.

4. Experimental Section

General Data

All reactions were routinely carried out under a nitrogen atmosphere, using standard Schlenk techniques or Glovebox. Glassware was oven dried before use. Solvents: dichloromethane (CH_2Cl_2), tetrahydrofuran (THF), diethyl ether (Et_2O), petroleum ether referring to a fraction of bp 60-80 °C, and acetonitrile (CH_3CN) were dried and distilled prior to use. Acetone was degassed and stored under inert atmosphere on molecular sieves. Other solvents such as ethylacetate (EtOAc), chloroform, ethanol (EtOH), methanol (MeOH), heptane, toluene, $CDCl_3$, D_2O, CD_3CN (Sigma Aldrich) were employed without further purification. NH_3BH_3 (ammonia–borane, Sigma Aldrich) was sublimated before use. Reagents: sodium tetraphenilborate and boron trifluoride diethyl ether were employed as purchased. Complex **1** was prepared as reported in the literature.[14a]

The NMR spectra were recorded using Varian Mercury Plus VX 400 (^{1}H, 399.9; ^{13}C, 100.6 MHz), Varian Inova 600 (^{1}H, 599.7; ^{13}C, 150.8 MHz) spectrometers at 298 K; chemical shifts were referenced internally to residual solvent peaks. Infrared spectra were recorded at 298 K on a Perkin-Elmer Spectrum 2000 FT-IR spectrophotometer. ESI-MS spectra were recorded on Waters Micromass ZQ 4000 with samples dissolved in MeOH or CH_3CN. Elemental analyses were performed on a Thermo-Quest Flash 1112 Series EA instrument. UV irradiation was performed by using a commercial Hg lamp (125 W).

AB Dehydrocoupling

In a typical experiment, a THF solution of AB (0.4 mL) was added to a NMR tube. A solution of the corresponding iron complex (0.1 mL) was added and the NMR tube sealed. For experiments that required heating, the NMR tube was placed in a heating block. For experiments that required photoactivation, the NMR tube was exposed to Hg-lamp (125 W). C_6D_6 was used as lock solvent. Reactions were monitored by ^{11}B-NMR, ^{11}B{^{1}H}-NMR, and ^{1}H-NMR.

Open-Vessel AB Dehydrocoupling

The same setup as for the general dehydrocoupling, but the NMR tube is left open inside a glovebox nitrogen atmosphere.

AB Dehydrocoupling in Sealed Glass Photoreactor

Catalytic dehydrogenation experiments were carried out using a sealed glass reactor (volume of 217 mL) equipped with a septum to collect the gases produced during reaction. The reactor temperature was maintained constant through an external jacket cooled with water, while the pressure was monitored using a digital pressure indicator (Figure S10, Supporting Information). The reactions were carried out under inert atmosphere using anhydrous THF as solvent (10−50 mL) maintained under vigorous stirring. After the dissolution of AB (1.1 mmol) and catalyst (5−25 mol%), the reactor was exposed to 325 nm UV irradiation. The reaction was monitored by periodically collecting gas samples (1.3 mL) from the reactor environment. H_2 and CO concentration were determined through offline GC analyses using Agilent 7890 A equipped with a thermal conductivity detector. The presented dynamic TOF values were calculated considering the experimental number of activated catalytic sites, corresponding to the amount of CO evolved during reaction:

$$\textit{For a certain reaction time: } TOF = H_2\ produced\ (mol/s)/CO\ measured\ (mol)$$

When a decrease in CO evolution was observed, catalyst activation was considered complete and TOF values were subsequently calculated considering the highest quantity of CO registered.

XRD Powder

The XRD powder analysis was carried out using a PANalytical X'Pert diffractometer equipped with a copper anode (Cu Kα,

$\lambda = 0.15418$ nm) and a fast X'Celerator detector. A 2θ range of 5°–80° was investigated, using a step size of 0.1° and a time per step of 2 s.

In-Situ FTIR Characterization

In situ FTIR experiments were carried out using a Bruker Tensor II instrument using a 1 mm thick CaF_2 cell specially modified to conduct photoinduced reaction with evolution of gaseous products; before the solution of interest, blanks were measured in the absence of the cell and in the sole presence of the solvent employed. A white LED lamp was used for irradiation; multiple measurements (every 30 s) of the same solution were acquired in order to study the behavior of the complex and the progress of the reaction over time. To the spectra recorded have been substracted depending on the circumstance: the spectrum of the solvent, the spectrum of the solution containing the complex, or the spectra acquired from complex and substrate recorded before switching on the led. In a general procedure the concentration of analytes was 0.0528M.

Synthesis of Cationic Iron Complexes 2 and 3: Dicarbonyl-(2,4-bis(trimethylsilyl)bicyclo[3.3.0]nona-1,4-Dienyl)(1,3-Dimethyl-Ilidene)Iron Trifluoromethanesulfonate (2)

Dicarbonyl-(2,4-bis(trimethylsilyl)bicycle-[3.3.0]nona-1,4-dien-3-one)[1,3-dimethyl-ilidene]iron complex (**1**) 0.020 g (0.035 mmol) was dissolved in 5 mL of diethyl ether under inert atmosphere. 3.3 µL of HCF_3SO_3 (solution at 98% in CH_2Cl_2) were subsequently added. The reaction mixture was stirred for 10 min at room temperature, then the precipitate obtained was filtered, washed with 10 mL of hexane and dried under vacuum. The yellow solid obtained was identified as **2** by IR, ^{1}H-NMR, ^{13}C-NMR, ^{19}F-NMR and ESI-MS. ^{1}H-NMR (399.9 MHz, $CDCl_3$) δ (ppm): 7.32(s, 2H, CH_{NHC}), 5.89 (s, 1H, -COH), 3.95 (s. 6H, -NCH_3), 2.39 (m, 4H, CH_2), 1.79 (m, 4H, CH_2), 0.29 (s, 18H, $CH_{3,TMS}$). ^{13}C-NMR (150.8 MHz, $CDCl_3$): δ (ppm) 213.8 (CO), 169.6 ($C_{carbene}$), 144.9 (C-OH), 126.6 (CH_{NHC}), 104.3 ($C_{2,5}$, Cp), 80.6 ($C_{3,4}$, Cp), 39.9 (-NCH_3), 23.7 (CH_2, Cp), 21.9 (CH_2, Cp), 0.01 (CH_3, TMS). ^{19}F-NMR (282.4 MHz, $CDCl_3$) δ (ppm): −79.10 (CF_3SO_3). IR (CH_2Cl_2, cm^{-1}): (νCO) 2023, 1973 cm^{-1}. ESI-MS (m/z): 486 [M^+], 149 [$CF_3SO_3^-$]. Anal. Calcd (%) for $C_{23}H_{34}O_6N_2F_3SSi2Fe$: C, 43.50; H, 5.39; N, 4.41. Found: C, 43.42; H, 5.43; N 4.38.

Synthesis of Carbonyl-(2,4-Bis(trimethylsilyl)bicyclo[3.3.0]nona-1,4-Dien-3-One)[1,3-Dimethylilidene][acetonitrile]iron Trifluoromethanesulfonate (3)

In a dried 50 mL Schlenk flask, 0.030 g (0.096 mmol) of dicarbonyl-(2,4-bis(trimethylsilyl)bicyclo[3.3.0]nona-1,4-dienyl)(1,3-dimethyl-ilidene)iron trifluoromethanesulfonate (**2**) was dissolved in acetonitrile (15 mL). The reaction solution was irradiated with a UV lamp (325 nm) at room temperature for 15 min. Then, the solvent was removed in vacuo and the red crude was washed with hexane several times. The product identified as **3** by IR, ^{1}H-NMR, ^{13}C-NMR, ^{19}F-NMR and ESI-MS was obtained in quantitative yield. ^{1}H-NMR (400 MHz, CD_3CN) δ(ppm): 7.26 (s, 2 H, CH_{NHC}), 5.15 (C-OH), 3.84 (s, 3 H, CH_3), 2 .68-2.25 (m, 4 H, CH_2), 1.60 (s, 3 H, $NCCH_3$), 1.42 (m, 4 H, CH_2), 0.26 (s, 9 H, CH_3,TMS), 0.19 (s, 9 H, CH_3,TMS); ^{13}C-NMR (150.8 MHz, CD_3CN) δ(ppm): 222.4 (CO), 179.9 ($C_{carbene}$), 171.1 (C_q,$NCCH_3$), 145.2 (C-OH), 126.4 (CH_{NHC}), 102.7, 96.4 75.5, 67.0 (C_q,Cp), 40.4 (NCH_3), 28.7, 24.9, 23.6, 22.5 (CH_2, Cp), 0.50, 0.30 (CH_3,TMS). ^{19}F-NMR (282.4 MHz, $CDCl_3$) δ (ppm): −151.28 (CF_3SO_3). ^{19}F-NMR (282.4 MHz, $CDCl_3$) δ (ppm): −78.30 (CF_3SO_3). IR (CH_2Cl_2, cm^{-1}): (νCO) 1950 cm^{-1}. ESI-MS (m/z): 499[$M]^+$, 149 [$CF_3SO_3^-$]. Anal. Calcd (%) for $C_{24}H_{37}O_5N_3F_3SSi_2Fe$: C, 44.48; H, 5.74; N, 6.48. Found: C, 44,59; H, 5.64; N 6.52.

Table 2. Crystal data and experimental details for 2.

Formula	$C_{23}H_{35}F_3FeN_2O_6SSi_2$
Fw	636.62
T, K	293(2)
λ, Å	0.71073
Crystal system	Orthorhombic
Space Group	$Pca2_1$
a, Å	18.3460(7)
b, Å	9.1757(4)
c, Å	18.0764(7)
Cell Volume, Å^3	3042.9(2)
Z	4
D_c, g cm^{-3}	1.390
μ, mm^{-1}	0.699
F(000)	1328
Crystal size, mm	0.15 × 0.13 × 0.11
θ limits, °	2.220–26.997
Index ranges	$-23 \le h \le 23$ $-11 \le k \le 11$ $-23 \le l \le 23$
Reflections collected	49 372
Independent reflections	6634 [$R_{int} = 0.0573$]
Completeness to θ max	100.0%
Data/restraints/parameters	6634/50/347
Goodness on fit on F^2	1.039
R_1 ($I > 2\sigma(I)$)	0.0412
wR_2 (all data)	0.1053
Largest diff. peak and hole, e Å^{-3}	0.528/−0.325

X-Ray Crystallography

Crystal data and collection details for **2** are reported in **Table 2**. The diffraction experiments were carried out on a Bruker APEX II diffractometer equipped with a PHOTON100 detector using Mo–Kα radiation. Data were corrected for Lorentz polarization and absorption effects (empirical absorption correction SADABS).[28] Structures were solved by direct methods and refined by full-matrix least-squares based on all data using F^2.[29] All hydrogen atoms were fixed at calculated positions and refined by a riding model, except the H-atom bonded to O(3) that was located in the Fourier difference map and refined isotropically. All nonhydrogen atoms were refined with anisotropic displacement parameters.

Acknowledgements

A.C. and N.S. contributed equally. The authors acknowledge the University of Bologna. R.M. and C.L. wish to acknowledge PRIN 2022 "Biomass-derived alcohols and polyols valorization and use by dehydrogenation/hydrogenation reactions promoted by bifunctional, proton-responsive homogeneous catalysts (ALCOVAL)" (20225N5T5B) financed by the European Union – Next Generation EU for financial support. A.C. and R.M. gratefully acknowledge Prof. Tom Baker for the beginning of this story and the fruitful discussion.

Open access publishing facilitated by Universita degli Studi di Bologna, as part of the Wiley - CRUI-CARE agreement.

Conflict of Interest

The authors declare no conflict of interest.

Data Availability Statement

The data that support the findings of this study are available in the supplementary material of this article.

Keywords: ammonia–borane dehydrocoupling · in situ infrared · N-heterocyclic carbene iron complexes · photoactivations

[1] European Commission e Directorate General for Communication, *REPowerEU, Joint European Action For More Affordable, Secure And Sustainable Energy*, Publications Office of the European Union **2022**
[2] a) Mission Innovation, *Clean Hydrogen*, [Online]. Available: https://explore.mission-innovation.net/mission/clean-hydrogen/; b) N. Schiaroli, M. Battisti, Patricia Benito, G. Fornasari, A. G. Di Gisi, C. Lucarelli, A. Vaccari, *Catalysts* **2022**, *12*, 109.
[3] a) US Department of Energy, *Hydrogen Shot*, [Online]. Available: https://www.energy.gov/eere/fuelcells/hydrogen-shot; b) N. Schiaroli, C. Lucarelli, M. C. Iapalucci, G. Fornasari, A. Crimaldi, A. Vaccari, *Catalysts* **2020**, *10*, 1345.
[4] Hydrogen Council, *Hydrogen Insights 2023 December Update*, [Online]. Available: https://hydrogencouncil.com/en/hydrogen-insights-2023-december-update/.
[5] a) D. Himmelbauer, F. Muller, C. Schweinzer, F. Casas, B. Pribanic, G. Le Corre, D. Thony, M. Trincado, H. Grutzmacher, *Chem. Commun.* **2024**, *60*, 885; b) P. Jurt, J. J. Gamboa-Carballo, C. Schweinzer, D. Himmelbauer, D. Thöny, T. L. Gianetti, M. Trincado, H. Grützmacher, *Dalton Trans.* **2024**, *53*, 14212; c) E. S. Osipova, E. S. Gulyaeva, E. I. Gutsul, V. A. Kirkina, A. A. Pavlov, Y. V. Nelyubina, A. Rossin, M. Peruzzini, L. M. Epstein, N. V. Belkova, O. A. Filippov, E. S. Shubina, *Chem. Sci.* **2021**, *12*, 3682; d) E. S. Gulyaeva, E. S. Osipova, S. A. Kovalenko, O. A. Filippov, N. V. Belkova, L. Vendier, Y. Canac, E. S. Shubina, D. A. Valyaev, *Chem. Sci.* **2024**, *15*, 1409; e) C. Peng, Y. Zhang, Y. Wang, W. Liu, Y. Yang, *Int. J. Hydrogen Energy* **2023**, *48*, 23633.
[6] a) G.-L. Li, A. Kumar Tripathi, H. Chan, S.-T. Chen, J.-T. Chang, T. Nakagawa, C.-Y. Wang, *ACS Sustainable Chem. Eng.* **2023**, *11*, 6143; b) A. Hajari, B. Roy, V. Kumar, A. Bishnoi, P. Sharma, *Chem. Select* **2021**, *6*, 1276; c) A. Hajari, B. Roy, P. Sharma, *Int. J. Hydrogen Energy* **2021**, *46*, 24214; d) S. Hausdorf, F. Baitalow, G. Wolf, F. O. R. L. Mertens, *Int. J. Hydrogen Energy* **2008**, *33*, 608; e) O. T. Summerscales, J. C. Gordon, *Dalton Trans.* **2013**, *42*, 10075; f) N. C. Smythe, J. C. Gordon, *Eur. J. Inorg. Chem.* **2010**, *4*, 509.
[7] T. B. Marder, *Angew. Chem., Int. Ed.* **2007**, *46*, 8116.
[8] S. Bhunya, T. Malakar, G. Ganguly, A. Paul, *ACS Catal.* **2016**, *6*, 7907.
[9] S. Bhunya; P. M. Zimmerman; A. Paul, *ACS Catal.* **2015**, *5*, 3478.
[10] V. Pons, R. T. Baker, N. K. Szymczak, D. J. Heldebrant, J. C. Linehan, M. H. Matus, D. J. Grant, D. A. Dixon, *Chem. Comm.* **2008**, 6597.
[11] a) A. Rossin, M. Peruzzini, *Chem. Rev.* **2016**, *116*, 8848; b) S. Todisco, L. Luconi, G. Giambastiani, A. Rossin, M. Peruzzini, I. E. Golub, O. A. Filippov, N. V. Belkova, E. S. Shubina, *Inorg. Chem.* **2017**, *56*, 4296; c) I. Ortega-Lepe, A. Rossin, P. Sánchez, L. L. Santos, N. Rendón, E. Álvarez, J. López-Serrano, A. Suárez, *Inorg. Chem.* **2021**, *60*, 18490; d) N. Schiaroli, L. Negahdar, M. Lützen, P. Hoang Ho, L. J. Allen, A. Natoli, F. Ospitali, F. Maluta, E. Rodríguez-Castellón, C. D. Damsgaard, G. Fornasari, A. M. Beale, P. Benito, *J. Catal.* **2023**, *424*, 140
[12] a) F. H. Stephens, V. Pons, R. T. Baker, *Dalton Trans.* **2007**, *25*, 2613; b) J. R. Vance, A. P. M. Robertson, K. Lee, I. Manners, *Chem Eur J.* **2011**, *17*, 4099; c) J. R. Vance, A. Schafer, A. P. M. Robertson, K. Lee, J. Turner, G. R. Whittell, I. Manners, *J. Am. Chem. Soc.* **2014**, *136*, 3048; d) P. Bhattacharya, J. A. Krause, H. Guan, *J. Am. Chem. Soc.* **2014**, *136*, 11153; e) A. Glüer, M. Förster, V. R. Celinski, J. Schmedt auf der Günne, M. C. Holthausen, S. Schneider, *ACS Catal.* **2015**, *5*, 7214; f) R. T. Baker, J. C. Gordon, C. W. Hamilton, N. J. Henson, P. H. Lin, S. Maguire, M. Murugesu, B. L. Scott, N. C. Smythe, *J. Am. Chem. Soc.* **2012**, *134*, 5598; g) A. M. Lunsford, J. H. Blank, S. Moncho, S. C. Haas, S. Muhammad, E. N. Brothers, M. Y. Darensbourg, A. A. Bengali, *Inorg. Chem.* **2016**, *55*, 964; h) N. T. Coles, M. F. Mahon, R. L. Webster, *Organometallics* **2017**, *36*, 2262; i) M. R. Elsby, K. Ghostine, U. K. Das, B. M. Gabidullin, R. T. Baker, *Organometallics* **2019**, *19*, 3844.
[13] a) F. Calcagno, C. Cesari, A. Gagliardi, A. Messori, A. Piazzi, F. Tamassia, M. Garavelli, F. Himo, R. Mazzoni, I. Rivalta, *Cell. Rep. Phys. Sci.* **2024**, *5*, 102291; b) A. Messori, G. Martelli, A. Piazzi, F. Basile, J. De Maron, A. Fasolini, R. Mazzoni, *Chempluschem* **2023**, *88*, 1; c) R. Mazzoni, C. Cesari, V. Zanotti, C. Lucarelli, T. Tabanelli, F. Puzzo, F. Passarini, E. Neri, G. Marani, R. Prati, F. Viganò, A. Conversano, F. Cavani, *ACS Sus. Chem. Eng.* **2019**, *7*, 224; d) C. Cesari, R. Mazzoni, E. Matteucci, A. Baschieri, L. Sambri, M. Mella, A. Tagliabue, F. Basile, C. Lucarelli, *Organometallics* **2019**, *38*, 1041; e) R. Mazzoni, A. Gabiccini, C. Cesari, V. Zanotti, I. Gualandi, D. Tonelli, *Organometallics* **2015**, *34*, 3228; f) A. Fasolini, G. Martelli, A. Piazzi, M. Curcio, J. De Maron, F. Basile, R. Mazzoni, *ChemCatChem* **2024**, *19*, e202400393.
[14] a) A. Cingolani, C. Cesari, S. Zacchini, V. Zanotti, M. C. Cassani, R. Mazzoni, *Dalton Trns.* **2015**, *44*, 19063; b) A. Cingolani, I. Gualandi, E. Scavetta, C. Cesari, S. Zacchini, D. Tonelli, V. Zanotti, P. Franchi, M. Lucarini, E. Sicilia, G. Mazzone, D. Nanni, R. Mazzoni, *Catal. Sci. And Tehn.* **2021**, *11*, 1407; c) A. Cingolani, V. Zanotti, S. Zacchini, M. Massi, P. V. Simpson, N. Maheshkumar Desai, I. Casari, M. Falasca, L. Rigamonti, R. Mazzoni, *Appl. Organomet. Chem.* **2019**, *33*, 4779.
[15] a) C. Cesari, A. Cingolani, C. Parise, S. Zacchini, V. Zanotti, M. C. Cassani, R. Mazzoni, *RSC Adv.* **2015**, *5*, 94707; b) C. Cesari, R. Mazzoni, H. Muller-Bunz, M. Albrecht, *J. of Organomet Chem.* **2015**, *793*, 256.
[16] H.-J. Knölker, E. Baum, H. Goesmann, R. Klauss, *Angew. Chem. Int. Ed.* **1999**, *38*, 2064.
[17] Y. Wang, B. Quillian, P. Wei, C. S. Wannere, Y. Xie, R. B. King, H. F. Schaefer, P. v. R. Schleyer, G. H. Robinson, *J. Am. Chem. Soc.* **2007**, *129*, 2412.
[18] D. P. Curran, A. Solovyev, M. M. Brahmi, L. Fensterbank, M. Malacria, E. Lacôte, *Angew. Chem. Int. Ed.* **2011**, *50*, 10294.
[19] C. Cesari, A. Gagliardi, A. Messori, N. Monti, V. Zanotti, S. Zacchini, I. Rivalta, F. Calcagno, C. Lucarelli, T. Tabanelli, F. Cavani, R. Mazzoni, *J. of Catal.* **2022**, *405*, 47.
[20] a) A. R. Ploszajski, M. Billing, N. T. Skipper, J. K. Cockcroft, *Chem. Commun.* **2019**, *55*, 8290; b) Y. Song, J. Wang, L. Chen, P. Yang, *J. of Lumin.* **2020**, *225*, 117325; c) P. Pei, M. Cannon, G. Quanb, E. Kjeang, *J. Mater. Chem. A* **2020**, *8*, 19050.
[21] a) M. R. Weismiller, S. Q. Wanga, A. Chowdhury, S. T. Thynell, R. A. Yetter, *Thermochimica Acta* **2013**, *551*, 110; b) S. Todisco, L. Luconi, G. Giambastiani, A. Rossin, M. Peruzzini, I. E. Golub, O. A. Filippov, N. V. Belkova, E. S. Shubina, *Inorg. Chem.* **2017**, *56*, 4296; c) J. D. Carpenter, B. S. Ault, *J. Phys. Chem.* **1991**, *95*, 3502.
[22] a) C. Zou, C. Zhang, B. Li, S. Wang, Z. Xie, Y. Song, *Mat. Sci. and Eng.: A* **2015**, *620*, 420; b) J.-s. Li, C.-r. Zhang, B. Li, F. Cao, Si-qing Wang, *Inorg. Chim. Acta* **2011**, *366*, 173
[23] S. F. Parker, *RSC Adv.* **2018**, *8*, 23875.
[24] V. D'Anna, A. Spyratou, M. Sharma, H. Hagemann, *Spectroch. Acta Part A: Molec. and Biomolec. Spect.* **2014**, *128*, 902.
[25] a) J. Baumann, F. Baitalow, G. Wolf, *Thermochimica Acta* **2005**, *430*, 9; b) A. Staubitz, A. Presa Soto, I. Manners, *Angew. Chem. Int. Ed.* **2008**, *47*, 6212; c) S. Todisco, L. Luconi, G. Giambastiani, A. Rossin, M. Peruzzini, I. E. Golub, O. A. Filippov, N. V. Belkova, E. S. Shubina, *Inorg. Chem.* **2017**, *56*, 4296
[26] a) M.-H. Chiang, V. Pelmenschikov, L. B. Gee, Yu-C. Liu, C.-C. Hsieh, H. Wang, Y. Yoda, H. Matsuura, Lei Li, S. P. Cramer, *Inorg. Chem.* **2021**, *60*, 555; b) V. Pelmenschikov, L. B. Gee, H. Wang, K. C. MacLeod, S. F. McWilliams, K. L. Skubi, S. P. Cramer, P. L. Holland, *Angew. Chem. Int. Ed.* **2018**, *57*, 9367; c) M. G. I. Galinato, C. M. Whaley, D. Roberts, P. Wang, N. Lehnert, *Eur. J. Inorg. Chem.* **2011**, 1147.
[27] a) Z. Lu, B. L. Conley, T. J. Williams, *Organometallics* **2012**, *31*, 6705; b) X. Zhang, L. Kam, R. Trerise, T. J. Williams, *Acc. Chem. Res.* **2017**, *50*, 86.
[28] G. M. Sheldrick *SADABS*, *Program For Empirical Absorption Correction*, University of Göttingen, Germany **1996**.
[29] G. M. Sheldrick, *SHELX97*, *Program For Crystal Structure Determination*, University of Göttingen, Germany **1997**.

Manuscript received: April 14, 2025
Revised manuscript received: May 25, 2025
Version of record online: June 16, 2025